EUROPEAN ORGANIZATION FOR NUCLEAR RESEARCH

Closing in on critical net-baryon fluctuations at LHC energies: cumulants up to third order in Pb–Pb collisions

ALICE Collaboration

Abstract

Fluctuation measurements are important sources of information on the mechanism of particle production at LHC energies. This article reports the first experimental results on third-order cumulants of the net-proton distributions in Pb–Pb collisions at a center-of-mass energy $\sqrt{s_{NN}} = 5.02$ TeV recorded by the ALICE detector. The results on the second-order cumulants of net-proton distributions at $\sqrt{s_{NN}} = 2.76$ and 5.02 TeV are also discussed in view of effects due to the global and local baryon number conservation. The results demonstrate the presence of long-range rapidity correlations between protons and antiprotons. Such correlations originate from the early phase of the collision. The experimental results are compared with HIJING and EPOS model calculations, and the dependence of the fluctuation measurements on the phase-space coverage is examined in the context of lattice quantum chromodynamics (LQCD) and hadron resonance gas (HRG) model estimations. The measured third-order cumulants are consistent with zero within experimental uncertainties of about 4% and are described well by LQCD and HRG predictions.

1 Introduction

Predictions based on the theory of the strong interaction, QCD, imply that, at sufficiently high energy densities, nuclear matter transforms into a state called quark–gluon plasma (QGP) [1, 2], where chiral symmetry is restored and quarks and gluons are deconfined. Ultrarelativistic heavy-ion collisions are ideal environments to study the phase diagram of strongly interacting matter and the physics of the QGP state as a function of temperature (T) and baryon chemical potential (μ_B). While the QCD phase diagram is largely unknown for $\mu_B > 450$ MeV, the region below that value down to $\mu_B = 0$ has been well explored theoretically [2, 3] and experimentally [4]. In that region, the chiral phase transition is most likely a continuous crossover with pseudo-critical temperature $T_{pc} \approx 157$ MeV at $\mu_B = 0$ [5, 6]. Near $\mu_B = 0$ the properties of the QCD phase transition depend on the number of quark flavors and their masses. For vanishing masses of the light quarks (u,d) the transition is of second order and belongs to the universality class of three-dimensional O(4)-symmetric spin models [7]. On the other hand, for the small physical quark masses this transition turns into a smooth crossover. To date, there is no experimental confirmation of the crossover nature of the transition. Moreover, the smallness of the physical quark masses may leave traces of critical behavior also for a continuous transition. Therefore, a significant effort at the RHIC and LHC colliders is concentrated on quantifying the nature of the phase transition in the small μ_B region.

For large μ_B the phase diagram may exhibit a "critical endpoint (CEP)". The search for the CEP is one of the main physics goals of the beam energy scan programs at RHIC [8, 9], at the CERN SPS [10], and at FAIR [11].

Recent LQCD [12–14] calculations of chiral susceptibilities for small quark masses exhibit a clear peak at T_{pc}, consistent with the chemical freeze-out temperature extracted by the analysis of hadron multiplicities [4, 15] measured in central Pb–Pb collisions by the ALICE experiment. This suggests that the chemical freeze-out occurs very close to the chiral phase transition at LHC energies. Critical signals associated with this phenomenon can be linked with long-range correlations and increasing multiplicity fluctuations due to the existence of the massless modes of the second-order phase transition [16, 17]. In particular, the fluctuations of the conserved charges are very sensitive probes for the equation of state and can be directly related to the thermodynamic susceptibilities, which are calculable in the framework of LQCD. The quark-number susceptibilities are defined as the derivatives of the reduced QCD pressure with respect to the reduced chemical potentials ($\hat{\mu} = \mu/T$) of the conserved charges

$$\chi_{klmn}^{B,S,Q,C} = \frac{\partial^{(k+l+m+n)}(P(\hat{\mu}_B, \hat{\mu}_S, \hat{\mu}_Q, \hat{\mu}_C)/T^4)}{\partial \hat{\mu}_B^k \partial \hat{\mu}_S^l \partial \hat{\mu}_Q^m \partial \hat{\mu}_C^n}\Big|_{\vec{\mu}=0}. \tag{1}$$

Here the relevant conserved charges, represented by the chemical potentials, are the electric charge Q, the baryon number B, the strangeness S, and the charm C. These susceptibilities are studied experimentally in terms of the ratios of the cumulants[1] of net-charge distributions [19]. Here and in the following, net-charge distribution stands for the difference between the distributions of positively and negatively charged particles, where "charge" refers to any additive quantum number. Signs of criticality due to the proximity of the chiral crossover transition to a second-order transition are expected to show up starting only with the sixth-order cumulants of net-charge distributions [16, 20]. Measuring conserved charge fluctuations in ultrarelativistic nuclear collisions is a challenging task, see Ref. [8] for a recent review. In addition to possible critical fluctuations due to the proximity of a CEP or O(N) criticality, there are several other dynamical signals, such as correlations due to baryon number conservation [21, 22], volume fluctuations [18], thermal blurring [23], resonance decays, which could overshadow the dynamical fluctuations of interest.

---

[1]The cumulants, κ_n, of net-baryon number, $\Delta N_B = N_B - N_{\bar{B}}$, are defined as the coefficients in the Maclaurin series of the logarithm of the characteristic function of ΔN_B [18].

The article is organized as follows. In Section 2, details are given about the ALICE detector, the data set and the analysis procedure, such as event and track selection criteria, particle identification and the efficiency correction technique. In Section 3, results on second-order cumulants of net-pion and net-kaon distributions are presented to demonstrate the influence of resonance decays on the measured cumulants. The main results are contained in the second- and third-order cumulants of net-proton distributions and compared to theoretical expectations. The article concludes, in Section 4, with a discussion on how the present results fit into the general strategy to get information on possible critical behaviour near the QCD phase boundary and with an outline of the next steps.

2   Experimental setup and data analysis

The measurements presented in this article are based on about 13 and 78 million minimum bias Pb–Pb collisions at $\sqrt{s_{\mathrm{NN}}} = 2.76$ and 5.02 TeV recorded with the ALICE detector [24, 25] in the years 2010 and 2015, respectively. Note that the running conditions have changed significantly in 2015. The details presented in this article refer only to the analysis of 2015 data (see Refs. [26, 27] for 2010). The minimum-bias trigger condition is defined by requiring a coincidence of hits in both V0 detectors [28] located on either side of the nominal interaction point along the beam direction and covering the pseudorapidity intervals $2.8 < \eta < 5.1$ and $-3.7 < \eta < -1.7$. The definition of the centrality [29] is based on the signal amplitudes measured in the V0 detectors, which are related to the collision geometry and the number of participating nucleons through a Monte Carlo (MC) simulation based on a Glauber model [30, 31]. Beyond event characterization, the main sub-detectors used in the analysis are the Time Projection Chamber (TPC) [32] for tracking and particle identification (PID), using the specific energy loss $\mathrm{d}E/\mathrm{d}x$, and the Inner Tracking System (ITS) [33, 34] for tracking and vertex determination.

Event and track selection criteria were applied to ensure optimal PID performance via $\mathrm{d}E/\mathrm{d}x$ measurement and momentum (p) resolution, as well as good track quality. The V0 [28] and the Zero Degree Calorimeter [35] timing information was used to reject background due to beam–gas interactions and parasitic beam–beam interactions. Along the beam direction, events occurring within ±0.15 cm, where tracking is affected by the central membrane of the TPC, and outside ±7 cm of the nominal interaction point were discarded to keep detection efficiency uniform as a function of event vertex position. The analysis uses tracks of charged particles reconstructed using the ITS and the TPC in the pseudorapidity range of $|\eta| < 0.8$ and with full azimuthal acceptance. In 2015, the TPC performance was affected by local space-charge distortions caused by the accumulation of space charge originating from the gaps between adjacent readout chambers [36]. Although these distortions are corrected on average during reconstruction, their fluctuations caused a significant mismatch between the TPC and ITS tracks. They affected all events detected within a time interval of about 0.5 seconds after a collision, corresponding to the full drift time of ions from the amplification region in the TPC readout chambers to the central electrode. Collisions within such time intervals were discarded using the event interaction time (timestamp) when also the mean matching efficiency between the TPC and ITS for all tracks in an event was less than 88% (the nominal TPC–ITS track matching efficiency is peaked at 90.5% with a small pseudorapidity and momentum dependence of a few percent). By applying this condition about 7% of all events are rejected. Tracks were accepted if they crossed at least 80 padrows out of a maximum of 159 and their χ^2 value per space point from the track fit is less than 3.5. To improve the $\mathrm{d}E/\mathrm{d}x$ resolution and reduce the contributions from track splitting[2], two additional track selection criteria were applied. The number of clusters used for the $\mathrm{d}E/\mathrm{d}x$ calculation[3] was set to more than 70. These criteria address both tracks crossing chamber boundaries and split tracks, both leading to a deterioration of the $\mathrm{d}E/\mathrm{d}x$ measurement. To suppress contributions from secondary particles from weak decays, the distance of closest approach

---

[2]Track splitting occurs when a track is reconstructed as two separate tracks due to poor $\mathrm{d}E/\mathrm{d}x$ resolution.

[3]Clusters that are very close to the TPC readout chamber boundaries [36] or are from overlapping tracks are not considered in the calculation of $\mathrm{d}E/\mathrm{d}x$. Therefore, the number of clusters used to calculate $\mathrm{d}E/\mathrm{d}x$ may differ from the number of clusters used for track selection. This quantity is particularly important for the $\mathrm{d}E/\mathrm{d}x$ resolution.

(DCA) of the extrapolated track to the primary vertex position was required to be less than 1 cm along the beam direction, while in the transverse plane a transverse momentum (p_T) dependent DCA selection of less than (0.018 cm $+ 0.035 p_T^{-1.01}$) with p_T in GeV/c was applied to account for the p_T dependence of the DCA resolution [37]. In addition, daughter tracks from reconstructed secondary weak-decay kink topologies were discarded.

In 2015, the ALICE TPC was operated at interaction rates up to 8 kHz during Pb–Pb collisions. These high interaction rates resulted in a possible pile-up of several interactions during the 90 μs drift time. The fraction of pile-up events, which occur within a few cm of the primary vertex, the so-called in-bunch pile-up, is less than 1‰ of the entire data set. Therefore, in-bunch pile-up has a negligible impact on the results. Moreover, in-bunch pile-up events were further suppressed thanks to the high-precision vertexing capabilities of the ITS. Even slightly displaced multiple vertices originating from interactions within the same bunch crossing can be discriminated. The much more frequent out-of-bunch pile-up events occur anytime during the drift time of the TPC, i.e., they are distributed equally along the time direction within the TPC and cannot be suppressed by reconstructed secondary vertices in the ITS. They lead to a significant deterioration in the measurements of the dE/dx of the triggered event caused by the baseline fluctuations in the TPC [36]. These pile-up events affect about 20% of the data collected in 2015 and are negligible for 2010. The resulting bias in the measured dE/dx is corrected to restore optimal PID performance and to avoid the need to discard events with pile-up [36].

Protons are identified by their dE/dx in the TPC and its known momentum dependence. To overcome the misidentification problem caused by overlapping dE/dx distributions for different particles, for instance at the crossings of kaons (K) and protons (p) or pions (π) and protons, a novel experimental technique, the Identity Method (IM) [38–40] was used. With this method, weights, which are obtained from the fits of dE/dx distributions, are assigned to each track reflecting the probability of a particle having a specific identity. Thereby all tracks can be kept without applying any selection on the PID variable and no second detector needs to be employed to identify the (anti)protons. In the present analysis, particles in the momentum range 0.6–2.0 GeV/c were retained. With particle identification based solely on the dE/dx measurements in the TPC, the efficiencies are independent of momentum in the selected range, and as high as about 91% for protons and about 83% for antiprotons. The difference of 8% is due to the absorption of antiprotons in the detector material. Both proton and antiproton detection efficiencies are nearly independent of collision centrality and are uniform within the kinematic acceptance used in this analysis. The cumulants of the net-proton distribution are reconstructed using the IM as well. Further details on the application of the IM to ALICE data are discussed in Ref. [27]. In Ref. [26], the method used here was applied to the analysis of second-order cumulants of net protons in Pb–Pb collisions at $\sqrt{s_{NN}} = 2.76$ TeV. The current analysis closely follows what is described there. The efficiency correction for the cumulants is performed by using proton and antiproton efficiencies in analytic formulas derived in Refs. [41–43] assuming efficiency losses governed by the binomial statistics (binomial efficiency loss). In order to ensure that this assumption is fulfilled, the ALICE detector response [25] was studied in detail with a full MC simulation using the HIJING event generator and the GEANT4 [44] transport software. The response of the TPC detector for the kinematic range used in this analysis is illustrated in the left panel of Fig. 1 as a correlation between the reconstructed (N_p^{rec}) and the generated (N_p^{gen}) number of protons, where the reconstructed protons are those detected in the active area of the detector, as well as satisfying the event and track quality criteria. The event and track selection plays a significant role in the shape of the TPC detector response. For example, as discussed above, they can reduce the contributions from track splitting, which causes correlated dE/dx measurements, and thus a deviation from a binomial detector response.

After detailed study and optimization of the event and track selection, only a slight deviation from the binomial loss is observed, as shown in the right panel of Fig. 1. A MC verification test was performed to estimate the impact of this deviation in the final results on the net-proton cumulant measurements. In this
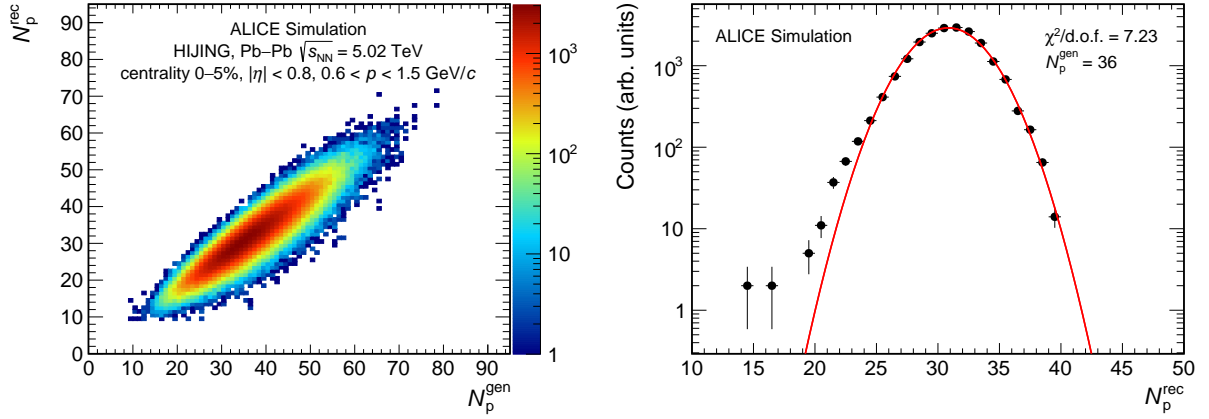
Figure 1: (Left) Correlation between the reconstructed ($N_{\mathrm{p}}^{\mathrm{rec}}$) and the generated ($N_{\mathrm{p}}^{\mathrm{gen}}$) number of protons for the most central Pb–Pb collisions simulated using the HIJING model [45]. (Right) Distribution of reconstructed proton number for a fixed value of $N_{\mathrm{p}}^{\mathrm{gen}} = 36$, where the fit demonstrates the deviation from a binomial efficiency loss.

MC closure test, particles are generated, including certain correlations such as the effect of baryon number conservation, and reconstructed after they have passed through the detector simulated with GEANT4. Then the efficiency correction is applied, and the generated and corrected observables are compared. The comparison is shown in Fig. 2 for the second- and third-order cumulant ratios of the net-proton distribution. The efficiency-corrected results obtained from the MC reconstructed data are in agreement with the results obtained from the MC generated data.
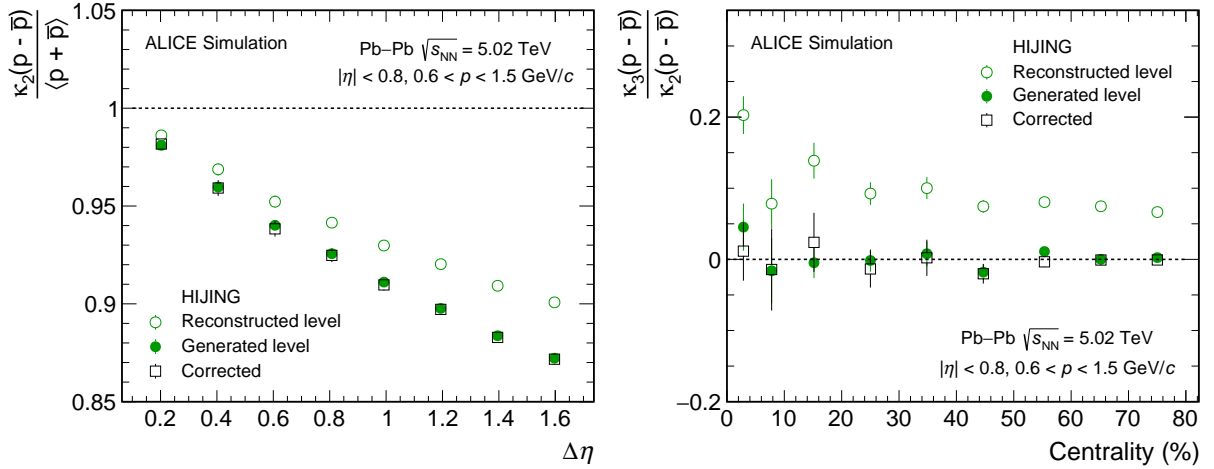

Figure 2: HIJING model [45] based calculations of the normalized second-order cumulants of net protons as a function of pseudorapidity window ($\Delta\eta$) (left) and ratio of third- to second-order cumulants (right) of net protons as a function of collision centrality at $\sqrt{s_{\mathrm{NN}}} = 5.02$ TeV. The results at the generated and reconstructed level are shown by the green closed and open circles, respectively. The error bars represent statistical uncertainties. The results after efficiency correction assuming binomial efficiency losses [41–43] are shown by black open squares.

The statistical uncertainties assigned to the reconstructed cumulants were determined using the subsample method as described in Ref. [27]. The fits to the measured $\mathrm{d}E/\mathrm{d}x$ distributions, which are the only inputs to the IM, are the dominant source of systematic uncertainty in the ratios of the cumulants, for both second and third order. The observed maximum deviation between fit variations [27] is 0.6% and 0.8% for the normalized second-order cumulants within the momentum intervals of 0.6–1.5 GeV/c and 0.6–2.0 GeV/c, respectively, and 4% for the ratio of third- to second-order cumulants in the momentum interval 0.6–1.5 GeV/c. The impact of possible imperfections in the $\mathrm{d}E/\mathrm{d}x$ correction procedure mentioned above is also included in this systematic uncertainty estimate by analyzing the data retaining

different fractions of events containing pile-up. The uncertainties associated with the detection efficiencies of the (anti)protons are also investigated by varying the detection efficiencies by an amount of $\pm 2\%$ for protons and antiprotons separately. The resulting systematic variation is less than 0.2% and 1.5% for the second- and third-order cumulants, respectively. Other sources of systematic uncertainty are estimated by varying the event and track selection criteria, resulting in a maximum uncertainty of less than 1%. The final total systematic uncertainty is obtained by adding in quadrature the individual maximum systematic deviations from these three groups of independent contributions. For the third-order cumulants, it varies between less than 0.5% for the most peripheral collisions and a maximum of 3% for the most central collisions for the pseudorapidity interval of $\Delta\eta = 1.6$.

3   Results

As potential candidates for conservation of electric charge and strangeness, results are reported for the pseudorapidity interval dependence of the second-order cumulants of net-pions and net-kaons produced in central Pb–Pb collisions.
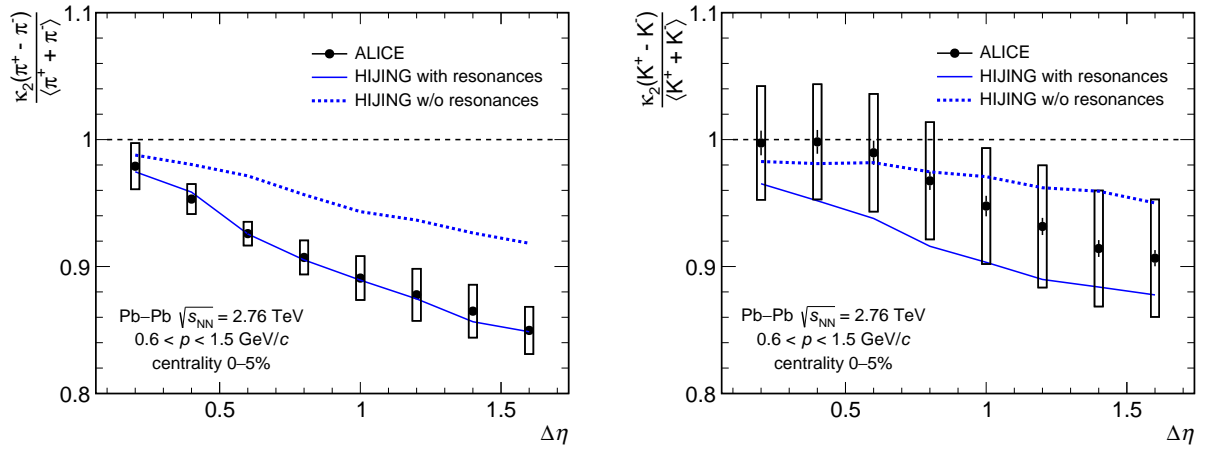

Figure 3: Pseudorapidity interval dependence of the second-order cumulants of net-pions (left) and net-kaons (right) normalized to the means (see text). The ALICE data are shown as solid black circles while the blue solid and dashed lines indicate the results from HIJING [45] model calculations with and without resonance contributions, respectively. The error bars represent statistical uncertainties and the boxes around the data points represent the total systematic uncertainties.

The observations in these channels are quite striking because they shed light on resonance decay contributions to fluctuations in Pb–Pb collisions at the LHC. Figure 3 shows the pseudorapidity interval dependence of the normalized second-order cumulants of net-pions and net-kaons compared with the results from HIJING [45] with and without resonance contributions. A significant effect of resonances, e.g., $\rho \to \pi^+\pi^-$ and $\phi \to K^+K^-$, is clearly visible in both cases. In fact, the decay of resonances into oppositely charged pion or kaon pairs drastically reduces the fluctuations and dominates the second-order cumulants of the respective net distributions. Therefore, to study the genuine electric charge and strangeness fluctuations, first a quantitative understanding of the resonance contributions is essential. On the other hand, there are no resonances that decay into p$\bar{\text{p}}$ with a sizeable branching ratio, therefore net-proton fluctuations are not obscured by this effect. It has been argued in the literature [46] that net-proton fluctuations are good proxies for net-baryon fluctuations, in particular for $\sqrt{s_{NN}} > 10$ GeV. Also, total electric-charge conservation is expected to have a negligible impact on the net-proton fluctuation measurements, since the electric charge is mostly carried by the charged pions, which are the most abundant species at LHC energies. The statistically independent Poisson limit for net-baryon distributions is the Skellam distribution, which is defined as the probability distribution of the difference of two random

variables, each generated from statistically independent Poisson distributions [47, 48]. For net protons, the nth-order cumulants of the Skellam distribution are given by

$$\kappa_n^{\text{Skellam}}(\mathrm{p} - \bar{\mathrm{p}}) = \langle \mathrm{p} \rangle + (-1)^n \langle \bar{\mathrm{p}} \rangle, \tag{2}$$

where $\langle \mathrm{p} \rangle$ and $\langle \bar{\mathrm{p}} \rangle$ are the mean values of the proton and antiproton multiplicity distributions, respectively. That means that even-order cumulants of the Skellam distribution of the net protons are just the sum of the mean numbers of protons and antiprotons. At LHC energies, these numbers are equal within 1% [49], and therefore the normalized cumulants of the Skellam distribution with respect to its second-order cumulant are zero for odd cumulants and unity for even cumulants. At T_{pc} [5, 6], both the predictions based on LQCD and the HRG [4] model agree with the Skellam baseline up to the third-order cumulants of the net protons, reflecting independent Poissonian fluctuations. The LQCD prediction [50], including the effect of dynamical quarks, shows a significant deviation from the Skellam baseline for the fourth- and higher-order cumulants, while the standard HRG does not contain such effects and deviations from the Skellam baseline are only due to baryon number conservation [51]. Fluctuations of conserved charges are meaningful only within a limited phase space. They vanish in the full phase space, in order to obey the conservation laws, and asymptotically approach the Poisson limit for very small acceptance, where dynamical correlations are suppressed [41]. Therefore, the fluctuations of net-baryons are studied in the framework of the Grand Canonical Ensemble, where the net-baryon number is conserved only on average. Accordingly, the analysis is performed differentially as a function of the collision centrality, the pseudorapidity interval, $\Delta \eta = 0.2$ to 1.6, and for two different momentum ranges, 0.6–1.5 GeV/c and 0.6–2.0 GeV/c. It should be noted that the determination of centrality and the net-proton analysis are based on measurements in different pseudorapidity intervals to avoid trivial effects due to autocorrelations [18].
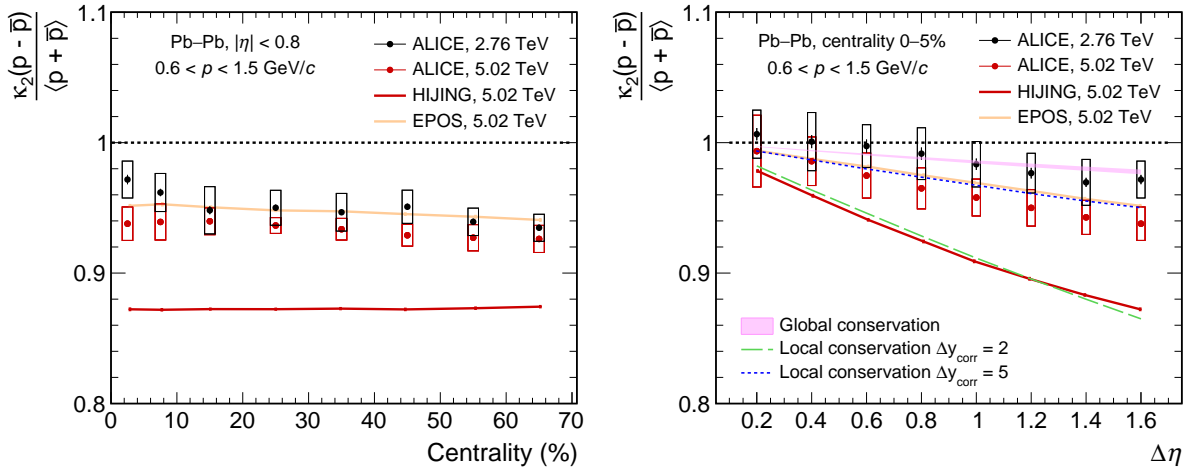

Figure 4: (Color online) Centrality (left) and pseudorapidity interval (right) dependence of the normalized second-order cumulants of net protons. The ALICE data are shown by black and red markers for $\sqrt{s_{\text{NN}}} = 2.76$ and 5.02 TeV, respectively, while the colored shaded areas indicate the results from HIJING [45] and EPOS [52] model calculations at $\sqrt{s_{\text{NN}}} = 5.02$ TeV. The Skellam baseline is shown by the horizontal dashed black line. In the right panel the expectation from global baryon number conservation is shown as a pink band and the dashed colored lines represent the predictions of the model with local baryon number conservation [22].

Figure 4 shows the measured centrality and pseudorapidity dependence of the normalized second-order cumulants of the net protons in Pb–Pb collisions for the two collision energies. The 5.02 TeV data appear to be somewhat lower, however the two data sets agree within systematic uncertainties. It should be noted that the systematic uncertainties exhibit a large degree of correlation from bin to bin, but between the two collision energies are essentially uncorrelated due to the different running conditions (collision

rate, gas mixture and space charge distortions in the TPC, etc.). The normalized second-order cumulants are independent of collision centrality and are reduced by about 5% from the Skellam baseline for the $\Delta\eta = 1.6$ interval (left panel). As a function of the width of the $\Delta\eta$ interval, the fluctuations are increasingly reduced. Due to the increasing relevance of baryon number conservation with larger acceptance, this is expected. For the narrowest interval, statistically independent Poissonian fluctuations are observed. The results are also compared to results from HIJING [45] and EPOS [52] model calculations at $\sqrt{s_{NN}} = 5.02$ TeV. HIJING treats nucleus–nucleus collisions as an independent superposition of nucleon–nucleon interactions and does not include phenomena such as equilibrium and collectivity. While in HIJING the hadronization is based on the Lund string fragmentation scheme, EPOS (version 1.99, tuned to LHC data) distinguishes between string segments in a collectively behaving central part ("core") with high energy density and those in a peripheral part ("corona") with lower energy density, more like in pp or p–A collisions.

It is noteworthy that the proton to antiproton ratio is poorly reproduced in both models: the ratio is 1.025±0.004 and 1.008±0.002 for EPOS and HIJING, respectively, while the value measured by ALICE in Pb–Pb collisions at $\sqrt{s_{NN}} = 2.76$ TeV is unity within experimental uncertainties [49]. This implies that the volume fluctuations for the second- and third-order cumulants are not negligible for the model calculations [18].

Both model calculations show second-order fluctuations independent of centrality, as do the experimental data. The results from the EPOS calculations agree within the uncertainties with the data both in terms of the centrality and the $\Delta\eta$ dependencies. The HIJING model results exhibit a 12% suppression compared to Poissonian fluctuations for the widest $\Delta\eta$ interval and are significantly below the data. This is also apparent in the dependence on the width of the $\Delta\eta$ interval (right panel of Fig. 4). The dependence on acceptance, and specifically the discrepancy between the HIJING results and the data, is examined in view of global vs local baryon number conservation modelled in Refs. [18, 22, 26, 51] using a canonical statistical model. The right panel of Fig. 4 shows the results for different widths of the correlation interval, ranging from global baryon number conservation to short-range correlations. As expected, measurements and model calculations converge to the Skellam baseline in the limit of very small acceptance. As already noted in Ref. [26], the data from ALICE indicate long-range rapidity correlations ($\Delta y_{corr} > 5$) between protons and antiprotons, therefore originating from the early phase of the collision [53]. Here $\Delta y_{corr}/2$ is defined as the correlation length between protons and antiprotons in rapidity [22], so that $\Delta y_{corr} = 5$ means that protons are correlated with antiprotons within 2.5 rapidity units into either direction.

The HIJING model calculations reflect a much smaller correlation length ($\Delta y_{corr} = 2$) than the EPOS model ($\Delta y_{corr} = 5$) and the ALICE data. This is likely due to the formation of baryons in string breaking in the underlying Lund string model [54]. This sensitivity to the range of proton–antiproton correlations is further studied by enlarging the momentum acceptance for the $\sqrt{s_{NN}} = 5.02$ TeV data. The resulting normalized second-order cumulants are shown in Fig. 5 for the momentum intervals 0.6–1.5 GeV/c and 0.6–2.0 GeV/c. Using the wider momentum interval the number of protons and antiprotons roughly doubles. While there is again no change with the collision centrality, the larger acceptance leads to a larger suppression of fluctuations for the wider momentum range. For the largest $\Delta\eta$ interval, the suppression amounts to an additional 4%. All calculations reflect the reduction in the fluctuations. However, while the magnitude is properly reproduced by the canonical statistical model predictions with a long correlation length [22], it can be noted that the suppression due to increased acceptance is somewhat weaker in the EPOS results. The HIJING calculations properly track the absolute reduction in fluctuations, but fall significantly below the data in absolute amount.

Figure 6 shows the centrality and pseudorapidity dependence of the ratio of third- to second-order cumulants of net protons at $\sqrt{s_{NN}} = 5.02$ TeV before and after the efficiency correction. The uncorrected results deviate from the Skellam baseline, which is set at zero, because the net-proton number is nonzero
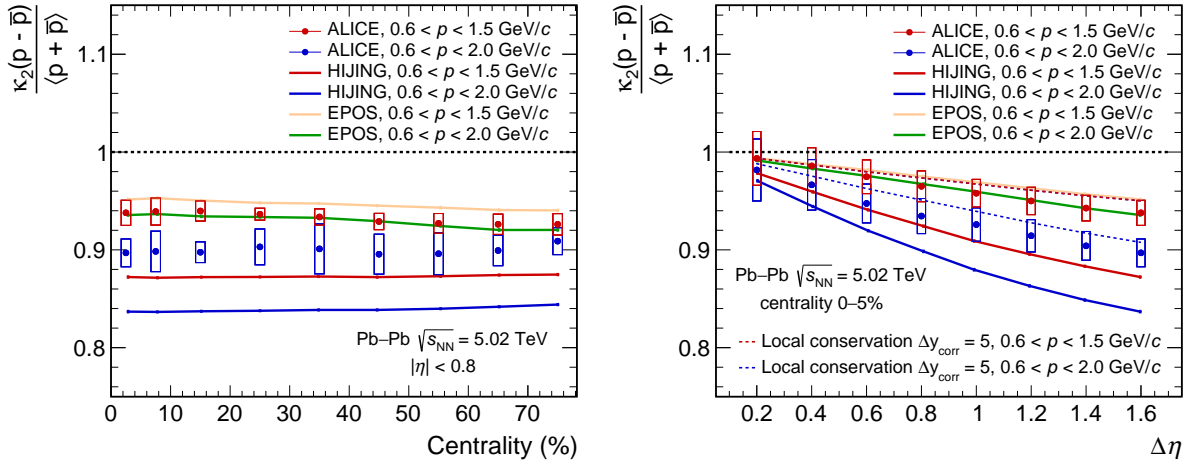
Figure 5: (Color online) Centrality (left) and pseudorapidity interval (right) dependence of the normalized second-order cumulants of net protons for $\sqrt{s_{NN}} = 5.02$ TeV and two momentum intervals for the protons. The ALICE data are shown by red and blue markers for $0.6 < p < 1.5$ GeV/c and $0.6 < p < 2.0$ GeV/c, respectively. The colored shaded areas indicate the results from the HIJING [45] and EPOS [52] model calculations. In the right panel, in addition, the dashed colored lines represent the predictions from the model with local baryon number conservation with $\Delta y_{corr} = 5$ [22].

due to antiproton absorption in the detector material and, to a smaller degree, by a proton knock-out contribution. Understanding and controlling the particle detection efficiency is one of the major technical challenges in the measurement of higher-order cumulants, since the efficiency enters into the analytical formula of the correction with the corresponding high power [41–43]. This affects both statistical and systematic uncertainties of the corrected data. Therefore, the final results depend crucially on a very accurate determination of the proton and antiproton efficiencies. Note that the efficiency correction approximately doubles the statistical uncertainties, as also noted in Ref. [55]. The experimentally achieved overall precision is better than 4% for the most central collisions and much smaller for more peripheral collisions.
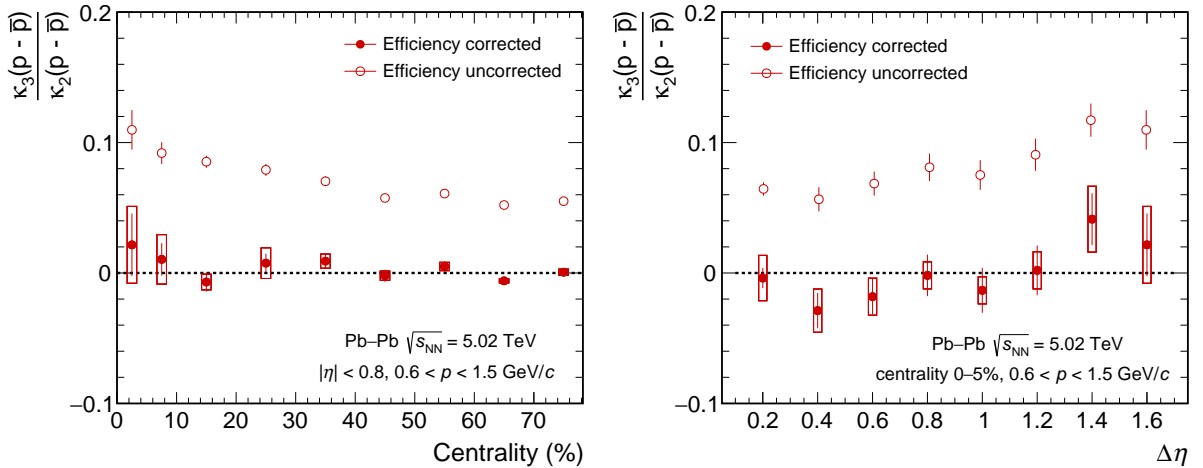

Figure 6: Centrality (left) and pseudorapidity interval (right) dependence of the ratio of third- to second-order cumulants for net protons at $\sqrt{s_{NN}} = 5.02$ TeV before (open markers) and after (closed markers) efficiency correction.

After efficiency correction, the data agree with the zero baseline within the experimental uncertainties, which is consistent with expectations from the HRG model. Note that in the HRG model all odd cumulants vanish at LHC energy, where the number of baryons and antibaryons agree. The odd cumulants

9

vanish under these conditions also if baryon number conservation is included, see Refs. [51, 56]. Also in LQCD [57] the odd cumulants vanish.

In Fig. 7, the third-order cumulant measurements are also compared with HIJING and EPOS model calculation results. Both models include baryon number conservation but, as mentioned above, the net-proton number is positive within the current experimental acceptance. Therefore, the resulting third-order cumulants for all centrality and pseudorapidity difference intervals shift toward positive values and are affected by the volume fluctuations [18] visible in the 10–20% centrality interval, where the centrality range doubles (left panel). The agreement of the experimental third-order cumulants with a value of zero is a confirmation that the average number of protons and antiprotons is the same at LHC energies and that the systematic uncertainties for these measurements are under good control.
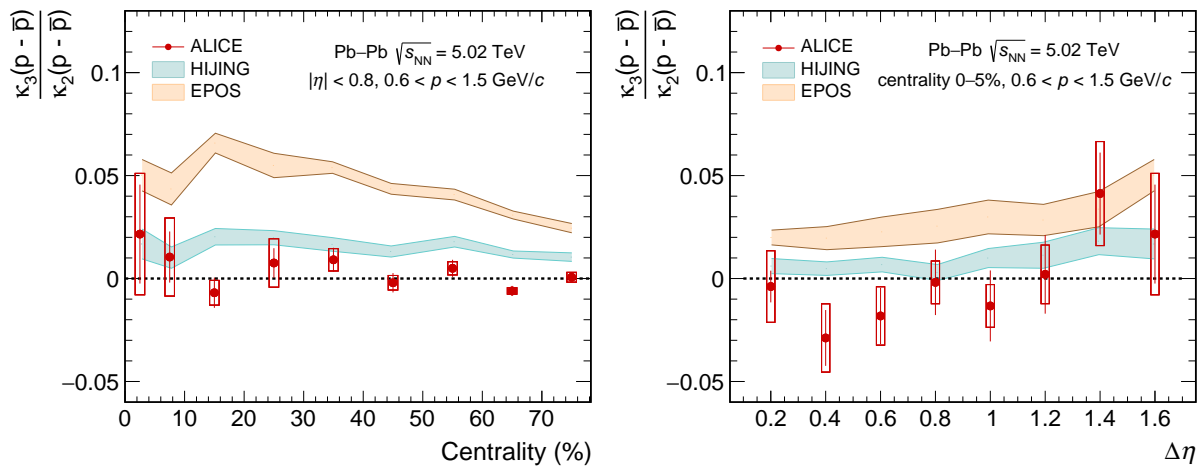

Figure 7: (Color online) Centrality (left) and pseudorapidity interval (right) dependence of the ratio of third- to second-order cumulants for net protons at $\sqrt{s_{\mathrm{NN}}} = 5.02$ TeV. The ALICE data are shown by red markers, while the colored shaded bands represent the results from HIJING [45] and EPOS [52] model calculations.

4   Conclusions

In summary, net-proton cumulant measurements up to third order and net-pion and net-kaon second-order cumulant measurements are reported. The technical challenges related to data analysis, in particular efficiency correction and event pile-up, could be overcome as discussed in detail. Resonance contributions prove to be challenging in the study of fluctuations of the net-electric charge and the net-strangeness. A deviation of about 4% from the Skellam baseline is observed for the second-order net-proton cumulants for the widest $\Delta\eta$ interval. Investigation of this deviation in light of baryon number conservation led to the conclusion that the 2010 data from ALICE [26] indicate the presence of long-range rapidity correlations between protons and antiprotons originating from the early phase of the collision. This finding is corroborated by the present analysis including the higher luminosity 2015 data with significantly different experimental conditions. Results of calculations using the HIJING generator, based on the Lund string model, reflect a much smaller correlation length of one unit of rapidity. This observed discrepancy calls into question the mechanism implemented in the Lund string model for the production of baryons. After accounting for the effect of baryon number conservation, the data from ALICE are consistent with LQCD expectations up to the third-order cumulants of the net protons. The finding of third-order net-proton cumulants consistent with zero with a precision of better than 4% is promising for the analysis of the higher-order cumulants during the operation of LHC with increased Pb–Pb luminosity [58] starting in 2022 and for the future heavy-ion detector planned for the early 2030s [59].

References

[1] E. V. Shuryak, "Quantum Chromodynamics and the Theory of Superdense Matter", *Phys. Rept.* **61** (1980) 71.

[2] H.-T. Ding, F. Karsch, and S. Mukherjee, "Thermodynamics of strong-interaction matter from Lattice QCD", *Int. J. Mod. Phys. E* **24** (2015) 1530007, `arXiv:1504.05274 [hep-lat]`.

[3] S. Borsanyi, Z. Fodor, C. Hoelbling, S. D. Katz, S. Krieg, and K. K. Szabo, "Full result for the QCD equation of state with 2+1 flavors", *Phys. Lett. B* **730** (2014) 99, `arXiv:1309.5258 [hep-lat]`.

[4] A. Andronic, P. Braun-Munzinger, K. Redlich, and J. Stachel, "Decoding the phase structure of QCD via particle production at high energy", *Nature* **561** (2018) 321, `arXiv:1710.09425 [nucl-th]`.

[5] **HotQCD** Collaboration, A. Bazavov *et al.*, "Chiral crossover in QCD at zero and non-zero chemical potentials", *Phys. Lett. B* **795** (2019) 15, `arXiv:1812.08235 [hep-lat]`.

[6] S. Borsanyi, Z. Fodor, J. N. Guenther, R. Kara, S. D. Katz, P. Parotto, A. Pasztor, C. Ratti, and K. K. Szabo, "QCD Crossover at Finite Chemical Potential from Lattice Simulations", *Phys. Rev. Lett.* **125** (2020) 052001, `arXiv:2002.02821 [hep-lat]`.

[7] R. D. Pisarski and F. Wilczek, "Remarks on the Chiral Phase Transition in Chromodynamics", *Phys. Rev. D* **29** (1984) 338.

[8] X. Luo and N. Xu, "Search for the QCD Critical Point with Fluctuations of Conserved Quantities in Relativistic Heavy-Ion Collisions at RHIC : An Overview", *Nucl. Sci. Tech.* **28** (2017) 112, `arXiv:1701.02105 [nucl-ex]`.

[9] N. Xu, "Exploration of the QCD Phase Diagram at Finite Baryon Density Region: Recent Results from RHIC Beam Energy Scan-I", *Springer Proc. Phys.* **203** (2018) 1.

[10] **NA49** Collaboration, T. Anticic *et al.*, "Search for the QCD critical point in nuclear collisions at the CERN SPS", *Phys. Rev. C* **81** (2010) 064907, `arXiv:0912.4198 [nucl-ex]`.

[11] **CBM** Collaboration, T. Ablyazimov *et al.*, "Challenges in QCD matter physics –The scientific programme of the Compressed Baryonic Matter experiment at FAIR", *Eur. Phys. J. A* **53** (2017) 60, `arXiv:1607.01487 [nucl-ex]`.

[12] **HotQCD** Collaboration, H. T. Ding *et al.*, "Chiral Phase Transition Temperature in (2+1)-Flavor QCD", *Phys. Rev. Lett.* **123** (2019) 062002, `arXiv:1903.04801 [hep-lat]`.

[13] S. Borsanyi, Z. Fodor, J. N. Guenther, S. K. Katz, K. K. Szabo, A. Pasztor, I. Portillo, and C. Ratti, "Higher order fluctuations and correlations of conserved charges from lattice QCD", *JHEP* **10** (2018) 205, `arXiv:1805.04445 [hep-lat]`.

[14] A. Bazavov *et al.*, "The chiral and deconfinement aspects of the QCD transition", *Phys. Rev. D* **85** (2012) 054503, `arXiv:1111.1710 [hep-lat]`.

[15] **ALICE** Collaboration, E. Abbas *et al.*, "Centrality dependence of the pseudorapidity density distribution for charged particles in Pb-Pb collisions at $\sqrt{s_{NN}}$ = 2.76 TeV", *Phys. Lett. B* **726** (2013) 610, `arXiv:1304.0347 [nucl-ex]`.

[16] B. Friman, F. Karsch, K. Redlich, and V. Skokov, "Fluctuations as probe of the QCD phase transition and freeze-out in heavy ion collisions at LHC and RHIC", *Eur. Phys. J. C* **71** (2011) 1694, `arXiv:1103.3511 [hep-ph]`.

[17] F. Parisen Toldin, A. Pelissetto, and E. Vicari, "The 3-D O(4) universality class and the phase transition in two flavor QCD", *JHEP* **07** (2003) 029, arXiv:hep-ph/0305264.

[18] P. Braun-Munzinger, A. Rustamov, and J. Stachel, "Bridging the gap between event-by-event fluctuation measurements and theory predictions in relativistic nuclear collisions", *Nucl. Phys. A* **960** (2017) 114, arXiv:1612.00702 [nucl-th].

[19] R. V. Gavai and S. Gupta, "Lattice QCD predictions for shapes of event distributions along the freezeout curve in heavy-ion collisions", *Phys. Lett. B* **696** (2011) 459, arXiv:1001.3796 [hep-lat].

[20] S. Ejiri, F. Karsch, and K. Redlich, "Hadronic fluctuations at the QCD phase transition", *Phys. Lett. B* **633** (2006) 275, arXiv:hep-ph/0509051.

[21] A. Bzdak, V. Koch, and V. Skokov, "Baryon number conservation and the cumulants of the net proton distribution", *Phys. Rev. C* **87** (2013) 014901, arXiv:1203.4529 [hep-ph].

[22] P. Braun-Munzinger, A. Rustamov, and J. Stachel, "The role of the local conservation laws in fluctuations of conserved charges", arXiv:1907.03032 [nucl-th].

[23] Y. Ohnishi, M. Kitazawa, and M. Asakawa, "Thermal blurring of event-by-event fluctuations generated by rapidity conversion", *Phys. Rev. C* **94** (2016) 044905, arXiv:1606.03827 [nucl-th].

[24] **ALICE** Collaboration, K. Aamodt *et al.*, "The ALICE experiment at the CERN LHC", *JINST* **3** (2008) S08002.

[25] **ALICE** Collaboration, B. B. Abelev *et al.*, "Performance of the ALICE Experiment at the CERN LHC", *Int. J. Mod. Phys. A* **29** (2014) 1430044, arXiv:1402.4476 [nucl-ex].

[26] **ALICE** Collaboration, S. Acharya *et al.*, "Global baryon number conservation encoded in net-proton fluctuations measured in Pb-Pb collisions at $\sqrt{s_{NN}} = 2.76$ TeV", *Phys. Lett. B* **807** (2020) 135564, arXiv:1910.14396 [nucl-ex].

[27] **ALICE** Collaboration, S. Acharya *et al.*, "Relative particle yield fluctuations in Pb-Pb collisions at $\sqrt{s_{NN}} = 2.76$ TeV", *Eur. Phys. J. C* **79** (2019) 236, arXiv:1712.07929 [nucl-ex].

[28] **ALICE** Collaboration, E. Abbas *et al.*, "Performance of the ALICE VZERO system", *JINST* **8** (2013) P10016, arXiv:1306.3130 [nucl-ex].

[29] **ALICE** Collaboration, B. Abelev *et al.*, "Centrality determination of Pb-Pb collisions at $\sqrt{s_{NN}} = 2.76$ TeV with ALICE", *Phys. Rev. C* **88** (2013) 044909, arXiv:1301.4361 [nucl-ex].

[30] C. Loizides, J. Nagle, and P. Steinberg, "Improved version of the PHOBOS Glauber Monte Carlo", *SoftwareX* **1-2** (2015) 13, arXiv:1408.2549 [nucl-ex].

[31] M. L. Miller, K. Reygers, S. J. Sanders, and P. Steinberg, "Glauber modeling in high energy nuclear collisions", *Ann. Rev. Nucl. Part. Sci.* **57** (2007) 205, arXiv:nucl-ex/0701025.

[32] J. Alme *et al.*, "The ALICE TPC, a large 3-dimensional tracking device with fast readout for ultra-high multiplicity events", *Nucl. Instrum. Meth. A* **622** (2010) 316, arXiv:1001.1950 [physics.ins-det].

[33] **ALICE** Collaboration, "ALICE Inner Tracking System (ITS): Technical Design Report", *CERN-LHCC-99-012* (1999) . http://cds.cern.ch/record/391175.

[34] **ALICE** Collaboration, K. Aamodt *et al.*, "Alignment of the ALICE Inner Tracking System with cosmic-ray tracks", *JINST* **5** (2010) P03003, `arXiv:1001.0502 [physics.ins-det]`.

[35] **ALICE** Collaboration, G. Dellacasa *et al.*, "ALICE technical design report of the zero degree calorimeter (ZDC)", *CERN-LHCC-99-005* (1999) . `https://cds.cern.ch/record/381433`.

[36] M. Arslandok, E. Hellbär, M. Ivanov, R. H. Münzer, and J. Wiechula, "Track Reconstruction in a High-Density Environment with ALICE", *Particles* **5** (2022) 84, `arXiv:2203.10325 [physics.ins-det]`.

[37] **ALICE** Collaboration, K. Aamodt *et al.*, "Suppression of Charged Particle Production at Large Transverse Momentum in Central Pb-Pb Collisions at $\sqrt{s_{NN}} = 2.76$ TeV", *Phys. Lett. B* **696** (2011) 30, `arXiv:1012.1004 [nucl-ex]`.

[38] M. Gazdzicki, K. Grebieszkow, M. Mackowiak, and S. Mrowczynski, "Identity method to study chemical fluctuations in relativistic heavy-ion collisions", *Phys. Rev. C* **83** (2011) 054907, `arXiv:1103.2887 [nucl-th]`.

[39] A. Rustamov and M. I. Gorenstein, "Identity method for the determination of the moments of multiplicity distributions", *Phys. Rev. C* **86** (2012) 044906, `arXiv:1204.6632 [nucl-th]`.

[40] M. Arslandok and A. Rustamov, "TIdentity module for the reconstruction of the moments of multiplicity distributions", *Nucl. Instrum. Meth. A* **946** (2019) 162622, `arXiv:1807.06370 [hep-ex]`.

[41] A. Bzdak and V. Koch, "Acceptance corrections to net baryon and net charge cumulants", *Phys. Rev. C* **86** (2012) 044904, `arXiv:1206.4286 [nucl-th]`.

[42] A. Bzdak and V. Koch, "Local Efficiency Corrections to Higher Order Cumulants", *Phys. Rev. C* **91** (2015) 027901, `arXiv:1312.4574 [nucl-th]`.

[43] T. Nonaka, M. Kitazawa, and S. Esumi, "More efficient formulas for efficiency correction of cumulants and effect of using averaged efficiency", *Phys. Rev. C* **95** (2017) 064912, `arXiv:1702.07106 [physics.data-an]`. [Erratum: Phys.Rev.C 103, 029901 (2021)].

[44] **GEANT4** Collaboration, S. Agostinelli *et al.*, "GEANT4–a simulation toolkit", *Nucl. Instrum. Meth. A* **506** (2003) 250–303.

[45] M. Gyulassy and X.-N. Wang, "HIJING 1.0: A Monte Carlo program for parton and particle production in high-energy hadronic and nuclear collisions", *Comput. Phys. Commun.* **83** (1994) 307, `arXiv:nucl-th/9502021`.

[46] M. Kitazawa and M. Asakawa, "Relation between baryon number fluctuations and experimentally observed proton number fluctuations in relativistic heavy ion collisions", *Phys. Rev. C* **86** (2012) 024904, `arXiv:1205.3292 [nucl-th]`. [Erratum: Phys.Rev.C 86, 069902 (2012)].

[47] P. Braun-Munzinger, B. Friman, F. Karsch, K. Redlich, and V. Skokov, "Net-charge probability distributions in heavy ion collisions at chemical freeze-out", *Nucl. Phys. A* **880** (2012) 48, `arXiv:1111.5063 [hep-ph]`.

[48] J. G. Skellam, "The frequency distribution of the difference between two Poisson variates belonging to different populations", *J. Royal Stat. Soc.* **A109(3)** (1946) 296.

[49] **ALICE** Collaboration, B. Abelev *et al.*, "Centrality dependence of π, K, p production in Pb-Pb collisions at $\sqrt{s_{NN}} = 2.76$ TeV", *Phys. Rev. C* **88** (2013) 044910, `arXiv:1303.0737 [hep-ex]`.

[50] A. Bazavov *et al.*, "Skewness, kurtosis, and the fifth and sixth order cumulants of net baryon-number distributions from lattice QCD confront high-statistics STAR data", *Phys. Rev. D* **101** (2020) 074502, `arXiv:2001.08530 [hep-lat]`.

[51] P. Braun-Munzinger, B. Friman, K. Redlich, A. Rustamov, and J. Stachel, "Relativistic nuclear collisions: Establishing a non-critical baseline for fluctuation measurements", *Nucl. Phys. A* **1008** (2021) 122141, `arXiv:2007.02463 [nucl-th]`.

[52] T. Pierog, I. Karpenko, J. M. Katzy, E. Yatsenko, and K. Werner, "EPOS LHC: Test of collective hadronization with data measured at the CERN Large Hadron Collider", *Phys. Rev. C* **92** (2015) 034906, `arXiv:1306.0121 [hep-ph]`.

[53] A. Dumitru, F. Gelis, L. McLerran, and R. Venugopalan, "Glasma flux tubes and the near side ridge phenomenon at RHIC", *Nucl. Phys. A* **810** (2008) 91, `arXiv:0804.3858 [hep-ph]`.

[54] B. Andersson, G. Gustafson, G. Ingelman, and T. Sjostrand, "Parton Fragmentation and String Dynamics", *Phys. Rept.* **97** (1983) 31–145.

[55] A. Pandav, D. Mallick, and B. Mohanty, "Effect of limited statistics on higher order cumulants measurement in heavy-ion collision experiments", *Nucl. Phys. A* **991** (2019) 121608, `arXiv:1809.08892 [nucl-ex]`.

[56] P. Braun-Munzinger, A. Rustamov, and J. Stachel, "Experimental results on fluctuations of conserved charges confronted with predictions from canonical thermodynamics", *Nucl. Phys. A* **982** (2019) 307, `arXiv:1807.08927 [nucl-th]`.

[57] **HotQCD** Collaboration, A. Bazavov *et al.*, "Skewness and kurtosis of net baryon-number distributions at small values of the baryon chemical potential", *Phys. Rev. D* **96** (2017) 074510, `arXiv:1708.04897 [hep-lat]`.

[58] Z. Citron *et al.*, "Report from Working Group 5: Future physics opportunities for high-density QCD at the LHC with heavy-ion and proton beams", *CERN Yellow Rep. Monogr.* **7** (2019) 1159, `arXiv:1812.06772 [hep-ph]`.

[59] **ALICE** Collaboration, "Letter of intent for ALICE 3: A next generation heavy-ion experiment at the LHC", *CERN-LHCC-2022-009, LHCC-I-038* (2022) . `http://cds.cern.ch/record/2803563`.